Journal of Physics Communications

PAPER

Interfacial charge transfer and Schottky barriers at c-Si/a-In heterojunctions

Piet Xiaowen Fang[1,2], **Stoyan Nihtianov**[1] , **Paolo Sberna**[1] , **Gilles A de Wijs**[2] and **Changming Fang**[3]

1   Electronic Instrumentation Lab, Faculty of Electrical Engineering, Mathematics and Computer Science, TU Delft, Mekelweg 4, 2628 CD Delft, The Netherlands
2   Radboud University, Institute for Molecules and Materials, Heyendaalseweg 135, NL-6525 AJ Nijmegen, The Netherlands
3   BCAST, Brunel University London, Uxbridge, Middlesex, UB8 3PH, United Kingdom

E-mail: Changming.Fang@brunel.ac.uk

Abstract

Metal-Semiconductor (M/S) heterojunctions, better known as Schottky junctions play a crucial role in modern electronics. At present, the mechanisms behind the M/S junctions are still a subject of discussion. In this work, we investigate the interfaces between semiconducting crystalline Si and amorphous metallic indium, Si{0 0 1}/a-In and Si{1 1 1}/a-In using both *ab initio* molecular dynamics simulations and a Schottky-Mott approach. The simulations reveal the formation of a distinct border between the Si substrates and amorphous In at the interfaces. The In atoms adjacent to the interfaces exhibit atomic ordering. Charge transfer occurs from In to Si, forming c-Si^{-q}/a-In^{+q} charge barriers at the interfaces. This indicates that a crystalline p-Si/a-In heterojunction will have rectifying properties, which agrees with an analysis using the Schottky-Mott model which predicts a Schottky barrier height of 1.3 eV for crystalline p-Si/a-In using the calculated work function for a-In (3.82 eV). We further discuss the interfacial charge transfer, related hole-depletion regions in Si adjacent to the interfaces and the Schottky-Mott approximations.

1. Introduction

In recent years, a novel heterojunction consisting of amorphous boron on crystalline silicon(c-Si/a-B) was prepared through deposition of amorphous B via decomposition of borane molecules, through a method named the PureB process. This device has been applied successfully in detection of near-ultraviolet (NUV) or vacuum ultraviolet (VUV) photons [1–4]. These new detectors are vital in pushing the frontier of nano-photolithography and nanoelectronics [1, 4]. The achievements reached through the PureB process open the path towards new Si-based heterojunctions/diodes for various applications [5–10], where the group III elements, aluminum (Al), gallium (Ga) and indium (In) are good candidates.

Indium (In) has advantages over the other elements in the same group [11, 12]. Due to its large atomic size, the possibility of alloying In and Si is restricted, contrasting Ga [13]. The elemental solid phase has a moderately high melting temperature, and thus it is possible to realize sharp c-Si/a-In heterojunctions via a moderate temperature process. Elemental indium solid is a metal and the c-Si/a-In heterojunction could potentially be used to create a Schottky diode which is formed by the junction of a semiconductor with a metal [5, 7, 14, 15].

Si-based Schottky diodes have several properties such as short switching time, temperature independence and low cut-in voltage [5, 7, 14], which make these devices particularly well-suited for applications requiring high sensitivity or efficiency, such as voltage clamping, blocking diodes or signal rectification [5, 7, 14, 15]. However, the exact mechanisms behind the rectifying effect of the crystalline-Silicon/Metal (c-Si/M) heterojunctions are still under discussion [5, 7, 14–17].

Recent *ab initio* molecular dynamics (AIMD) simulations for the c-Si/a-B interfaces revealed the formation of a distinct border between c-Si and a-B [18–20]. Charge transfer occurs from the interfacial Si to the B atoms, which gives rise to the formation of Si^{+q}/B^{-q} barriers. A hypothesis for the rectifying junction formation was

proposed in [18] based on this principle. In this model, the positively charged Si atoms induce the formation of an electron depleted region in the n-Si substrate interfacing with the amorphous B surface, which leads to the observed rectifying effect of the c-Si/a-B heterojunctions. However, fundamental questions naturally arose in this line of inquiry: (1) Besides B, is such junction formation possible using different elements or materials? (2) Can the newly proposed junction formation mechanism form a basis for a general theory behind Schottky junctions? Studying the c-Si/a-In junction is a starting point to address these questions.

There have been both experimental and theoretical investigations, mainly focused on the geometry and properties of the In sub- or thin-layer on Si{1 1 1} surfaces [21–28], mainly motivated by the discovery of unusual superconductivity [25]. In particular, Migitaka and Tokuyama reported a way to prepare diodes with good rectifying properties by alloying In with p-type Si [29]. The latter experiments also stimulate our interest in c-Si/In junctions.

On the other hand, theoretical approaches—especially parameter-free AIMD and first-principles methods —have also been applied to investigate the interfaces/heterojunctions between crystalline silicon and metals [7, 14–17, 30–32]. For example, in the 1970s, Louie *et al* investigated the interface between crystalline silicon and Al using density-functional theory (DFT) within the local density approximation (LDA) and observed interfacial states in the Si gap [31, 32]. Recently, there are more theoretical studies focusing on two-dimensional (2D) S/M heterojunctions [33, 34]. However there have been few recent theoretical studies on the interfaces between Si and In up to now.

Here we present a systematic study of the interfaces between Si{0 0 1} and Si{1 1 1} with a-In (c-Si/a-In) created using AIMD simulations. Wafers for these Si surfaces are commercially available and both interfaces exhibit different surficial geometry and chemical bonding [35]. The simulations produce a distinct border between the c-Si and a-In. The a-In atoms adjacent to the substrate exhibit atomic ordering. Electronic structure calculations reveal charge transfer from the interfacial In to Si, forming a charge barrier. We also calculate the work-functions for the In surfaces which are used to build the Schottky barrier for the c-Si/a-In junctions. The obtained information here is not only useful to get insight into the novel c-Si/a-In junctions, for furthering the design of new applicable heterojunctions, but also sheds some light on the c-Si/M heterojunctions in a more general way [14–17, 36, 37].

We first introduce the designs of the amorphous In surfaces and the c-Si/a-In interface systems, as well as the AIMD simulation and computation details in section 2. In section 3.1 we introduce the calculated crystal and electronic properties of the elemental solids Si and In. Then, in section 3.2 we present the interfacial chemical bonding at the equilibrated c-Si/a-In interfaces. The related electronic structure and interfacial charge transfer are both presented in section 3.3. The surficial structure and work functions of In{0 0 1}, In{1 0 0} and a-In surfaces are presented in section 3.4. In section 4, we build a band-alignment model for the c-Si/a-In junction based on the Schottky-Mott theory with the calculated work-function for a-In surfaces. We analyze the role of charge transfer at the c-Si/a-In interfaces on formation of hole-depletion regions at the p-Si substrates and its relation to the Schottky-Mott approximation. Finally we summarize the results in section 5.

2. Methods

The AIMD approach employs periodic boundary conditions. We utilized supercells for simulations of the c-Si/ a-In interfaces. For Si{0 0 1}/a-In, a tetragonal supercell with axis length $a = 3a_0$ (a_0 is the lattice parameter of cubic Si) was used for the in-plane axis. For Si{1 1 1}/a-In, a hexagonal supercell with $a = 2\sqrt{2}\,a_0$ was applied. The lengths of the c-axes were determined by the thickness of the crystalline Si slab and the number of the In atoms. The supercells for AIMD simulations are summarized in table 1. The supercells for the Si{0 0 1}/a-In and the Si{1 1 1}/a-In interfaces contain 444 atoms (144 Si and 300 In) and 492 atoms (192 Si and 300 In) respectively. These large supercells are required in order to avoid interaction between the Si surfaces and to minimize the risk of artificial crystallization of the melt during simulations [38, 39].

Apart from the c-Si/a-In systems, we also prepared a c-Si/c-In system, with the interface perpendicular to the *c*-axis of both crystals. The experimental lattice parameter at room temperature for cubic Si is $a = 5.4310$ Å [12]. For tetragonal In, the lattice parameters are $a = 3.2516\,Å, c = 4.9471$ Å [12]. Thus, it is possible to design a supercell with a pseudo-tetragonal lattice using $a = 3a_{Si} \approx 5a_{In}$. The length of the *c*-axis is determined by the Si (9 atomic layers) and In atoms (6 atomic layers). The optimized lattice parameters and numbers of Si and In atoms are included in table 1.

For the AIMD simulations of the interfaces we utilized the first-principles code VASP (Vienna *ab initio* Simulation Package) [40]. The code is based on a pseudo-potential plane-wave approach within density-functional theory (DFT) [40] and employs the projector augmented-wave (PAW) method [41, 42]. It allows variable fractional occupation numbers, which works well for interfaces between semiconductors and metals [40]. The AIMD simulation employs finite-temperature density-functional theory of the one-electron states,

Table 1. Input parameters of the c-Si/a-In and Si{0 0 1}/In{0 0 1} interfaces and c-In and a-In surfaces for the AIMD simulations/first-principles calculations.

System	Lattice	Unit params (Å)			Num. atoms		# dangling bonds for surf. atoms	Special feats.
		a	b	c	N_{Si}	N_{In}		
In{1 0 0} surf.	Orth.	47.54	3.33	4.88	—-	16	3[b]	Vac: 24.5 Å
In{0 0 1} surf.	Tet.	3.33	3.33	57.57	—-	13	4[b]	Vac: 19.0 Å
a-In surf.	Tet.	16.40	16.40	50.00	—-	300	3–5[b]	Vac: 30.0 Å
Si{0 0 1}/In{0 0 1}	Tet.	16.33[a]	16.33[a]	28.01	162	160	2[c]	
Si{1 1 1}/a-In	Hexa.	15.51	15.51	58.22	192	300	1[c]	
Si{0 0 1}/a-In	Tet.	16.40	16.40	41.35	144	300	2[c]	

Notes.

[a] The optimized lattice parameters.

[b] No. of lost bonds of surficial In.

[c] No. of lost bonds of surficial Si.

where the exact energy minimization and calculation of the exact Hellmann-Feynman forces occurs after each MD step using the preconditioned conjugate techniques, and the Nosé dynamics for generating a canonical NVT ensemble [40]. The generalized gradient approximation (GGA-PBE) was used for the exchange-correlation terms [43]. For the first-principles calculations we used cut-off energies of 350.0 eV for the wave functions and 500.0 eV for the augmentation charge density, which are higher than the corresponding default cut-off energies (E_{nmax}/E_{naug} = 95.9 eV/237.1 eV for In and 245.3 eV/322.07 eV for Si, respectively). We employed dense k-meshes, e.g. $4 \times 4 \times 2$ k-mesh (14 k-points) in the Brillouin zone (BZ) of the Si{0 0 1}/In{0 0 1} interface using the Monkhorst–Packmethod [44], whereas for the AIMD simulations of the large supercells, we employed a smaller cut-off energy (250.0 eV) and only the Γ-point in the BZs. The latter is due to the lack of periodicity of the whole systems in such crystal/amorphous interfaces [38, 39].

    We created amorphous In samples by equilibrating the systems at 3000 K for 2000 time-steps (1.5 fs per time-step, in total lasting 3 ps) after which the systems were cooled to the desired temperature. The obtained amorphous In (a-In) samples were placed on the Si substrates (c-Si), forming c-Si/a-In interfaces for the following AIMD simulations. We adopted a two-step approach here. First, the c-Si/a-In systems were allowed to equilibrate at 1000 K with the substrate Si atoms pinned. Next, all the atoms including the substrate were allowed to relax at 500 K for a period of time, followed by a second relaxation period at 300 K over 6 ps. This multiple-step approach helps to avoid collective movements of the atoms in the supercells.
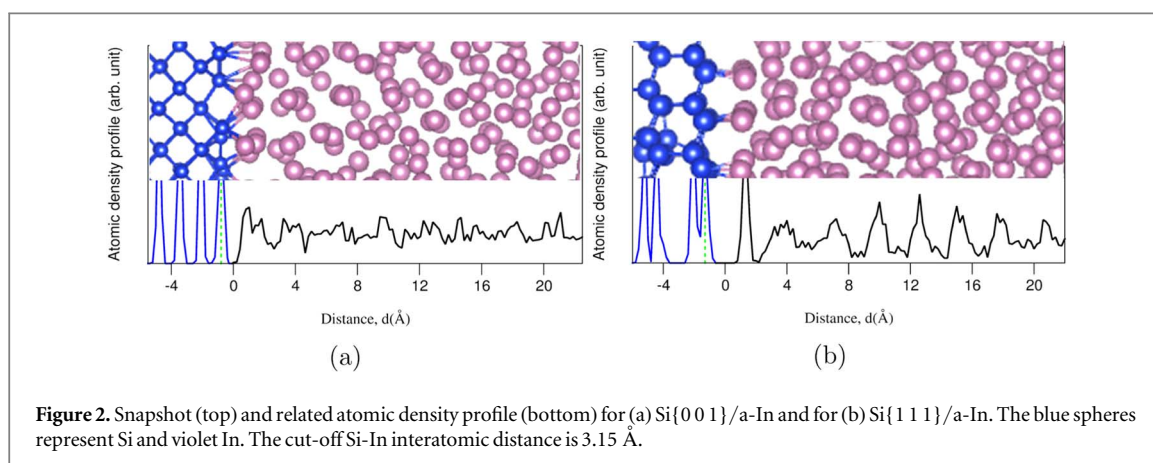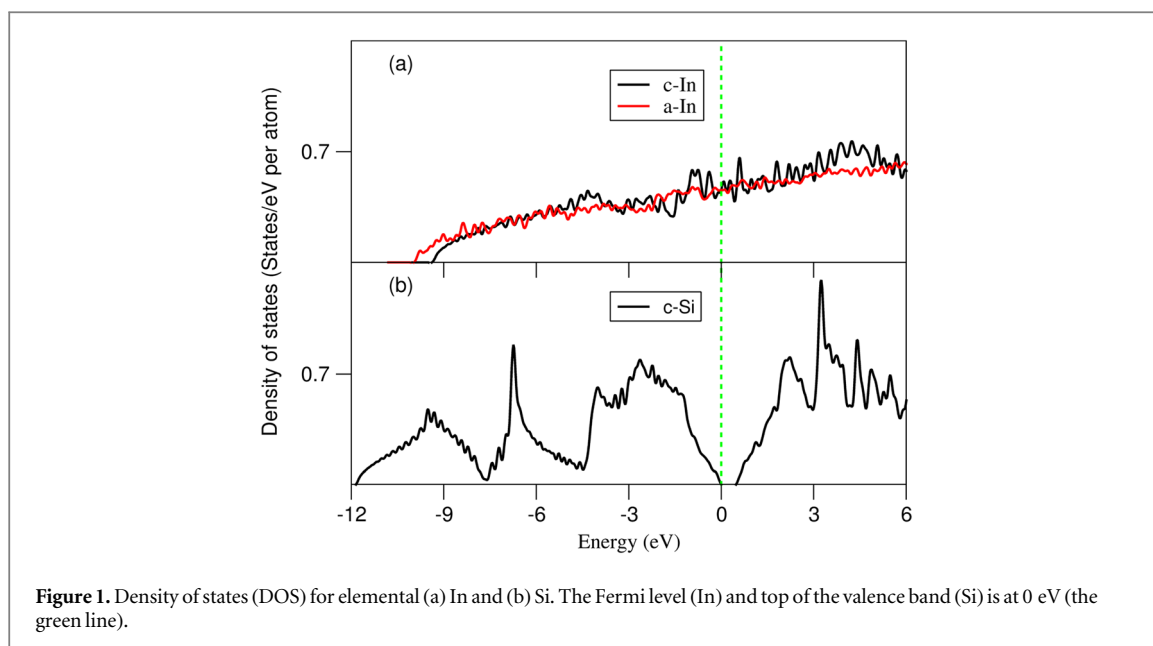
3. Results

3.1. Cohesive properties of Si and In

We first report first-principles structure optimizations for the elemental solids. The calculated lattice parameter for Faced-Centered Cubic (FCC) Si [45] is a = 5.469 Å, and for Body-Centered Tetragonal (BCT) c-In [12, 45] the axis lengths are a = 3.328 Å and c = 5.023 Å. The calculated values reproduced the experimental data in the literature, a = 5.43099 Å for Si and a = 3.32516 Å and c = 4.9471 Å for c-In at room temperature respectively [12]. Si was calculated to be a semiconductor with an indirect gap of 0.61eV (figure 1) when using the GGA-PBE approach. This value is notably smaller than the experimental value (1.17 eV) [46]. Such over- and under-estimations of respectively the lattice parameters for crystals and of the energy gaps for semiconductors/insulators are not unusual for the results of DFT-GGA calculations [43, 47].

    Figure 1(a) shows the density of states (DOS) curves for the crystalline and amorphous In. For both curves the general trends are similar and the DOS increases with energy. At the Fermi level, the densities are rather high, ~0.45 states/eV per In atom for both c- and a-In. This indicates that In is a free-electron-like metal and the electrons move freely in both c-In and a-In, although there is strong scattering due to local structural disorder in the latter. Figure 1(a) also shows that the bottom of the valence band for a-In is at about −9.9 eV, about 0.6 eV lower than that of c-In. Such lowering in energy for the states in a-In comes from the short In-In bonds in a-In.

3.2. Interfacial interaction at c-Si/a-In

During the AIMD simulations at 1000 K, the nearby liquid In atoms move to the pinned Si substrates. Correspondingly, there is very notable variation in total energies of these systems. At about 1 ps, the liquid In atoms form kinetically stable configurations. The total-electron energies of the c-Si/a-In systems become

Figure 1. Density of states (DOS) for elemental (a) In and (b) Si. The Fermi level (In) and top of the valence band (Si) is at 0 eV (the green line).

Figure 2. Snapshot (top) and related atomic density profile (bottom) for (a) Si{0 0 1}/a-In and for (b) Si{1 1 1}/a-In. The blue spheres represent Si and violet In. The cut-off Si-In interatomic distance is 3.15 Å.
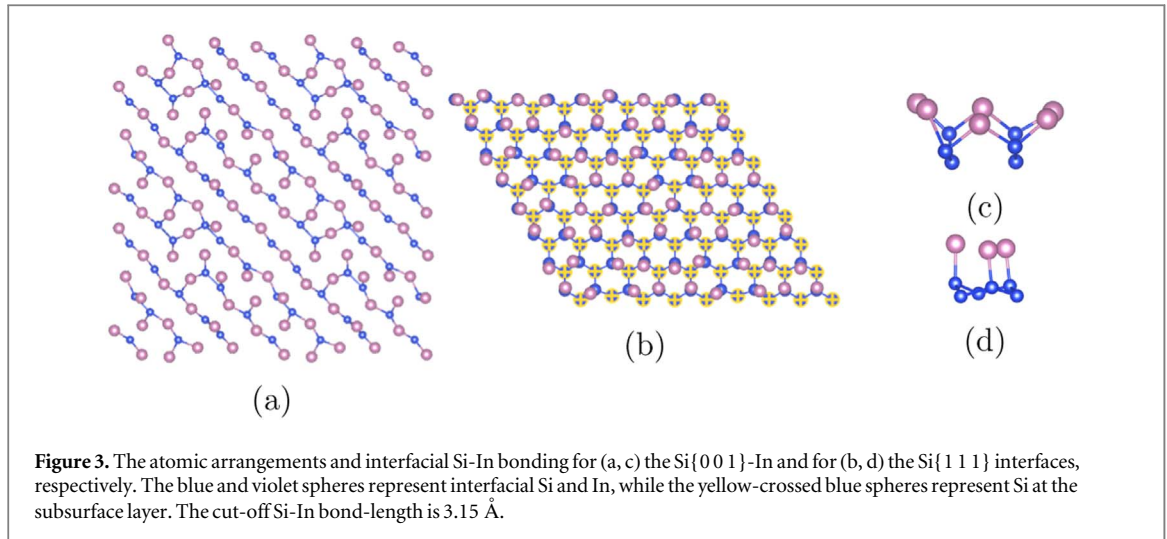
stabilized within 1 ps at 300 K with all the atoms fully relaxed. The thermally equilibrated structures of the c-Si/a-In interfaces are shown in figure 2.

For both Si{0 0 1}/a-In and Si{1 1 1}/a-In interfaces there is a clear separation between the c-Si substrates and the a-In. A closer look at figure 2 reveals a number of differences:

(i) The surficial Si atoms at the Si{1 1 1}/a-In interface resemble the structures found in the bulk (Figure 2(b)), whereas the surficial Si atoms in Si{0 0 1}/a-In display displacements from the ideal positions (figure 2(a));

(ii) The spacing between the c-Si substrate and a-In for Si{1 1 1}/a-In ($\sim$2.6 Å) is larger than that for Si{0 0 1}/a-In ($\sim$1.7 Å);

(iii) The surficial Si atoms at the Si{0 0 1}/a-In interface are coordinated primarily by two In atoms and two Si (Figure 2(a)), whereas the surficial Si atoms for Si{1 1 1}/a-In are coordinated by one In and three Si at the substrate (figure 2(b)).

These phenomena originate from the fact that Si prefers tetragonal coordination (sp^3 hybridization [48]) and the a-In atoms compensate the loss of the surficial Si atoms [35]. Figure 2 also shows variation of a-In distribution along z-direction, which is referred as atomic layering [39, 49].

To have a quantitative assessment of the layering phenomenon, we draw the atomic density profile $\rho(z)$ in figure 2 which is defined as follows [49, 50]:

Figure 3. The atomic arrangements and interfacial Si-In bonding for (a, c) the Si{0 0 1}-In and for (b, d) the Si{1 1 1} interfaces, respectively. The blue and violet spheres represent interfacial Si and In, while the yellow-crossed blue spheres represent Si at the subsurface layer. The cut-off Si-In bond-length is 3.15 Å.

$$\rho(z) = \frac{\langle N_z(t) \rangle}{L_x L_y \Delta z} \tag{1}$$

where L_x and L_y are respectively the in-plane x and y dimensions of the cell, and z the dimension perpendicular to the interface, Δz is the bin width, and $N_z(t)$ is the number of atoms between $z - (\Delta z/2)$ and $z + (\Delta z/2)$ at time t. $\langle N_z(t) \rangle$ represents a time-averaged number of atoms during the simulation.

As shown in figure 2, the layering phenomenon is moderate for Si{0 0 1}/a-In with the 1st a-In layer mostly splitting off from the 2nd layer In. This layering is more pronounced at Si{1 1 1}/a-In with a sharp In layer adjacent to the substrate, indicating that the substrate surface has strong influences on the atomic ordering in the amorphous In atoms adjacent to the substrates.

In figure 3 we show the atomic arrangements of the interfacial Si and In atoms at Si{0 0 1}/a-In (Figures 3(a) and 3(c)) and the Si{1 1 1}/a-In (figures 3(b) and 3(d)).

Figures 2(b) and 3(b) show that the surficial Si atoms are arranged similar to their pristine Si surface at the Si{1 1 1}/a-In interface. This is due to the strong chemical confinement from the sub-surface Si atoms. The In atoms in the layer closest to the Si{1 1 1} surface are positioned exclusively around the tops of the surficial Si. In fact, statistics from the atomic density profile (figures 2 and 3) revealed that the ratio of the number of In atoms at the 1st peak to that of the surficial Si atoms is 1:1.05, close to an even split.
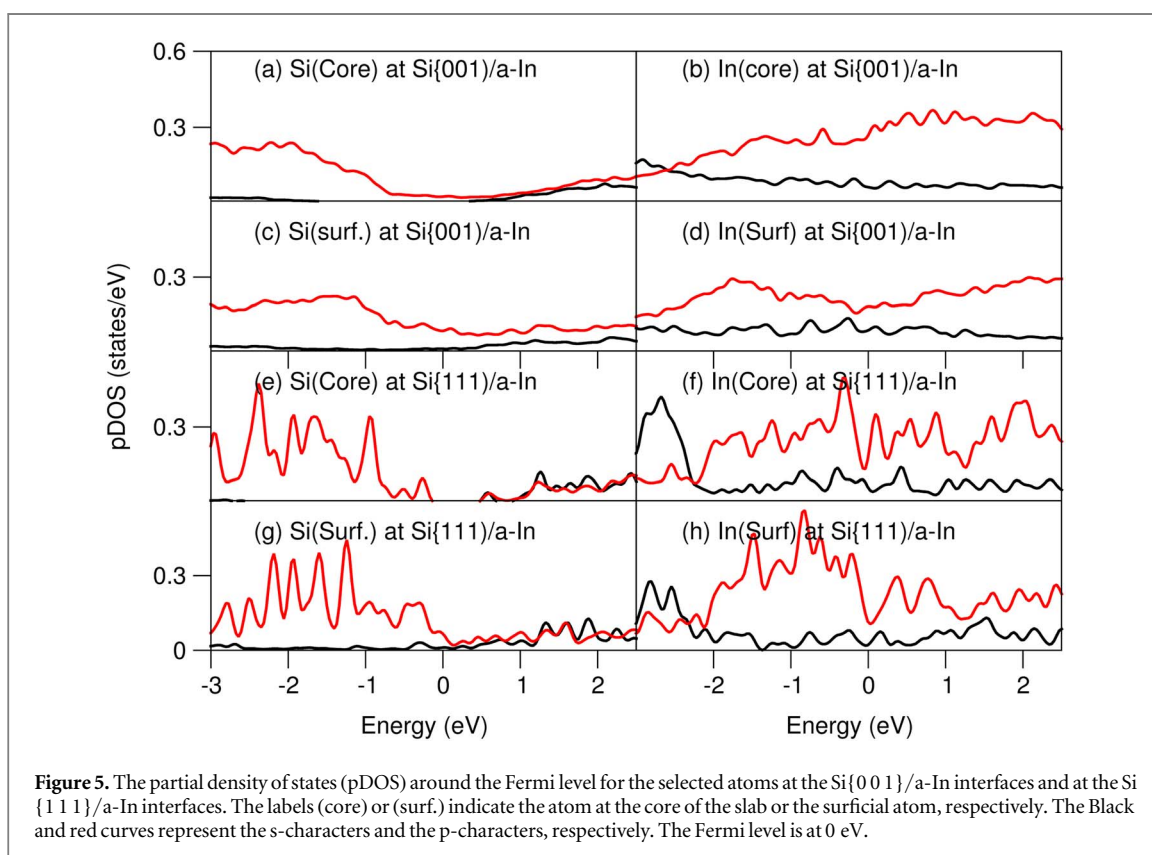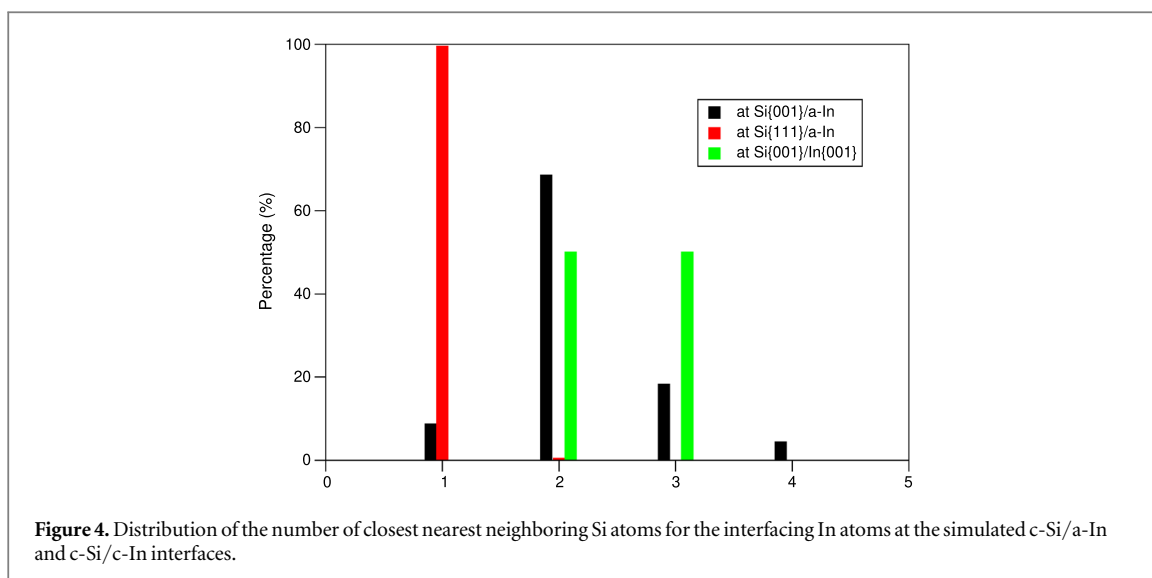
The few reconstructed Si-Si pairs (figure 3(a)) are similar to the surficial Si-Si clustering phenomenon observed experimentally at the pure Si{0 0 1} surfaces [35] and those induced by foreign atoms [51–53]. The In atoms closest to the Si{0 0 1} are distributed at various sites: the In is either at the middle of two Si atoms or around the tops of the surface Si atoms. Each surficial Si atom is connected predominantly to two In atoms. We found the ratio between the number of the surficial Si atoms and that of the bonded In atoms to be about 1:1.42, notably larger than the ratio found for the Si{1 1 1}/a-In interface, although the density of the surficial Si atoms at the former is just 15 percent smaller than that at the latter. To obtain statistically meaningful results, we analyzed over 20 configurations with the results plotted in figure 4.

The interfacial Si atoms at Si{1 1 1}/a-In are connected exclusively to one In neighbor (99.5%) (figure 4), satisfying the sp³ hybridization for Si according to Pauling's bonding theory [48]. The majority of the interfacial Si atoms at Si{0 0 1}/a-In (70%) have two In neighbors which are in a distorted tetragonal coordination. For the Si{0 0 1}/a-In interface roughly 20% and 10% of the interfacial Si atoms have three and one In neighbors, respectively. Such behavior at the interfaces is well aligned with the weaker structural confinement of the subsurface Si to the surficial Si atoms at Si{0 0 1}.

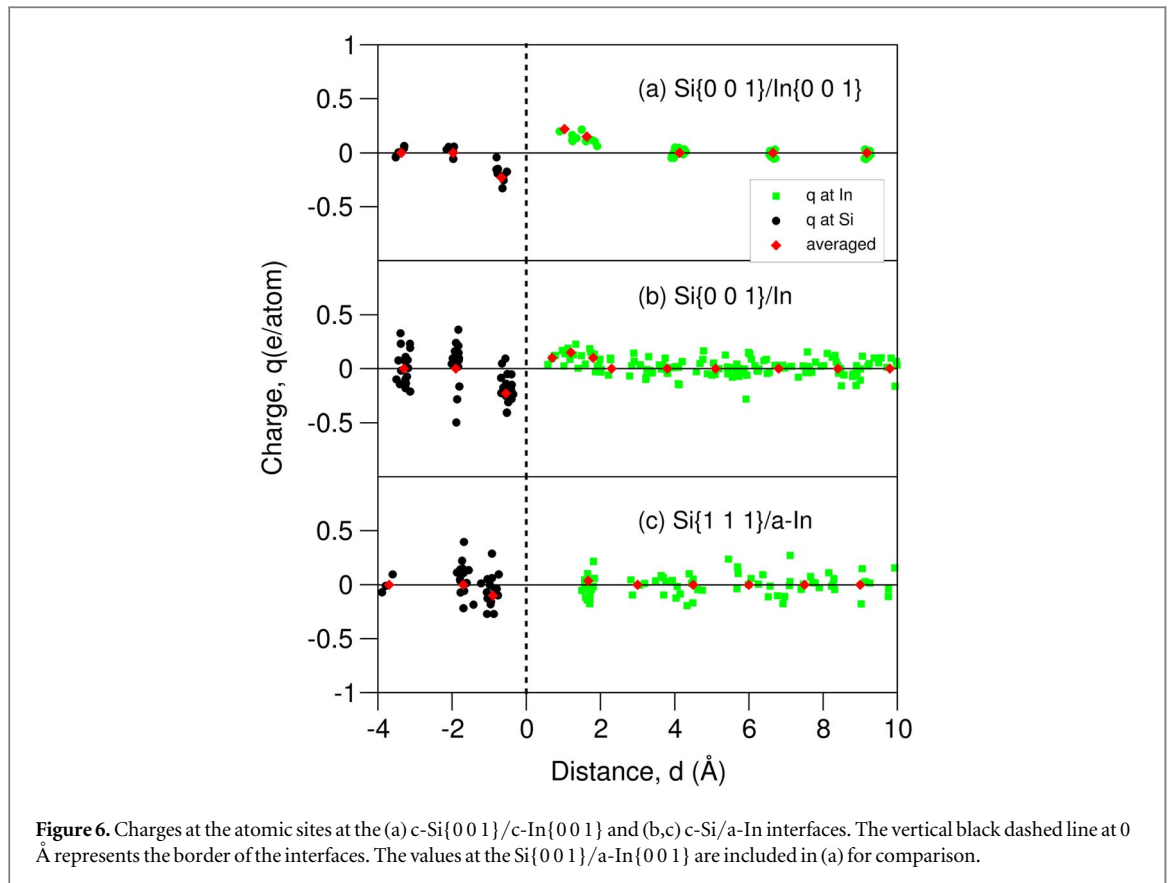### 3.3. Electronic structure and charge transfer at the c-Si/a-In interfaces

We performed electronic band structure calculations for the c-Si/a-In interfaces. In figure 5 the partial density of states (pDOS) is shown for selected atoms.

The electronic band structure calculations showed that for the DOS of the Si{0 0 1}/a-In interface, the total DOS (tDOS) increases with energy from the bottom ranging from -12.0 to -1.5 eV. Then, it decreases to the Fermi level (0 eV), where a valley is found between 0.0 to 0.7 eV and the tDOS curve increases afterwards again with increasing energy (figure 5). The pDOS curves showed that there is no or little density of states at the gap of the core Si (figures 5(a), (e)). The weak pDOS at the core Si for the Si{0 0 1}/a-In interface originates from the local structural distortion and tails from the neighboring distorted Si atoms, as we showed before that the surficial Si atoms are strongly distorted at this interface. The free-electron nature of a-In is also reflected in the

Figure 4. Distribution of the number of closest nearest neighboring Si atoms for the interfacing In atoms at the simulated c-Si/a-In and c-Si/c-In interfaces.

Figure 5. The partial density of states (pDOS) around the Fermi level for the selected atoms at the Si{0 0 1}/a-In interfaces and at the Si {1 1 1}/a-In interfaces. The labels (core) or (surf.) indicate the atom at the core of the slab or the surficial atom, respectively. The Black and red curves represent the s-characters and the p-characters, respectively. The Fermi level is at 0 eV.

DOS curves of a-In for Si{1 1 1}/a-In (Figure 5), with the exception of the interfacial In bonded to Si (Figures 5(c), (g)), the latter of which shares similarities with the pDOS of interfacial Si (figures 5(c), (d)). This is understandable considering orbital hybridization between Si 3s, 3p and In 5s, 5p. Figure 5(a) and g show that the substrate Si atoms exhibit more semiconducting nature which is only weakly influenced by the interfacial Si-In interaction.

Additionally, we analyzed the dispersion curves of band structure along the BZ in-plane directions (not shown here). In the Si gap ranges (0.0 to 0.6 eV) there are many states mainly originating from metallic a-In with some minor contribution from interfacial Si-In. These results correspond well to those at the DOS curves, indicating a Schottky nature for these junctions. These states are similar to the Metal Induced Gap States (MIGS) at the Si{1 1 1}/Al interfaces [31, 32, 37]. The Fermi level of c-Si/a-In is at the energy position of Si relating to Fermi level alignments.

Figure 6. Charges at the atomic sites at the (a) c-Si{0 0 1}/c-In{0 0 1} and (b,c) c-Si/a-In interfaces. The vertical black dashed line at 0 Å represents the border of the interfaces. The values at the Si{0 0 1}/a-In{0 0 1} are included in (a) for comparison.

To obtain more direct information about the interfacial interactions, we analyse the charges at the atomic sites and charge transfer between the interfacial atoms. This information was obtained by employing the Bader's charge analysis approach [53] based on the calculated electronic density distributions at the c-Si/a-In and Si{0 0 1}/In{0 0 1} interfaces. Our calculations also show the obtained charges at the interfaces found in figure 6.

The charges at the Si sites near the interfaces correspond to scattering at c-Si/a-In interface, whereas the charges at the Si{0 0 1}/In{0 0 1} are shown to be more unified. The former phenomenon is due to the local bonding distortions induced by the interfacial a-In atoms. However, the averaged charges at the atomic sites at the Si{0 0 1}/a-In and Si{0 0 1}/In{0 0 1} are close to each other. The averaged interfacial charge transfer is −0.23 e/Si at the Si{0 0 1}/In interfaces and −0.08 e/Si for Si{1 1 1}/a-In. The charge transfer occurring from the interfacial In to Si at the c-Si/a-In interfaces is different from that at the c-Si/a-B interfaces where charge is transferred from the interfacial Si to B [19]. Further, the amounts of charge transfer at the Si{0 0 1}/a-A (A = In, B) interfaces are larger than for the corresponding Si{1 1 1}/a-A interfaces. This is due to the {0 0 1} interface having more Si-A interfacial bonds compared to the {1 1 1} interface [19], as shown in figures 2 and 4. The difference in charge sign at the c-Si/a-In and c-Si/a-B further indicates different mechanisms of rectification.

3.4. Work functions of In

For a Si/M heterojunction, the electrical properties, including rectification, are largely determined by the work function of the metal and Si [5, 7, 14–17, 37]. We performed calculations on the local potential and Fermi level for In{0 0 1} and In{1 0 0} and additional four different amorphous samples. Here we report the local relaxation and work functions for the crystalline and amorphous In surfaces.

The structural optimizations showed that there is moderate structural relaxation at the In{0 0 1} surface. The space between surficial and sub-surficial In atoms is just 0.3% different from that in the bulk. Meanwhile, strong local relaxation occurs at the In{1 0 0} surfaces: the space between the surficial and sub-surficial In atoms shrinks about 2.0%, while the space between the third and sub-surficial layers shrinks 1.3% and the space between fourth and third In layer expands 0.9%. From the fifth layer on, the layer-spacing becomes nearly the same as that of the bulk. Such notable difference in local structures between In{0 0 1} and In{1 0 0} originates from the higher atomic density at In{0 0 1} (0.095 Å^{-2}) compared to In{1 0 0} (0.062 Å^{-2} atom) (figures 7(a) and 7(d)). Moreover, the surficial In atoms at the {0 0 1} surface have four dangling bonds, whereas those at In{0 0 1} lose only three neighbors as shown in table 1. Analysis also showed that at the a-In surfaces, each surficial In atom loses three to five neighbors (table 1).
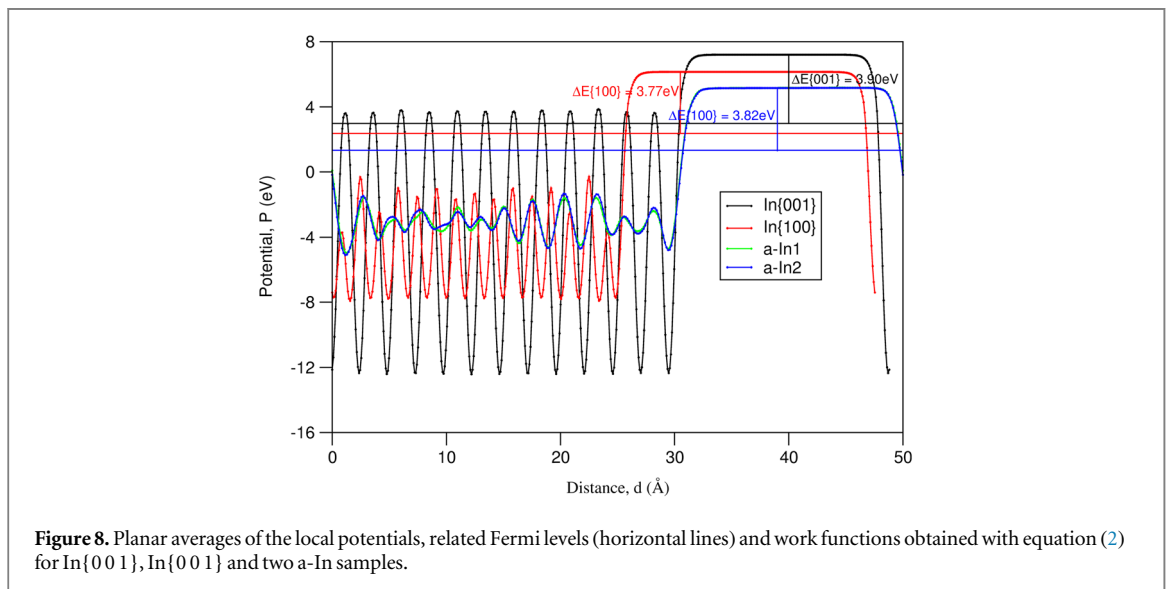
Figure 7. Electron density distribution with iso-surfaces (1.0×10^{-5} e/Å^3 at the outer skin of the slab) for (a) c-In{1 0 0}, (b) a-In, and (c) In{0 0 1} surfaces. The silvery spheres represent In atoms. The electron density decreases from red to yellow, to green to sky-blue and ends at dark yellow (iso-surfaces).

Figure 8. Planar averages of the local potentials, related Fermi levels (horizontal lines) and work functions obtained with equation (2) for In{0 0 1}, In{0 0 1} and two a-In samples.
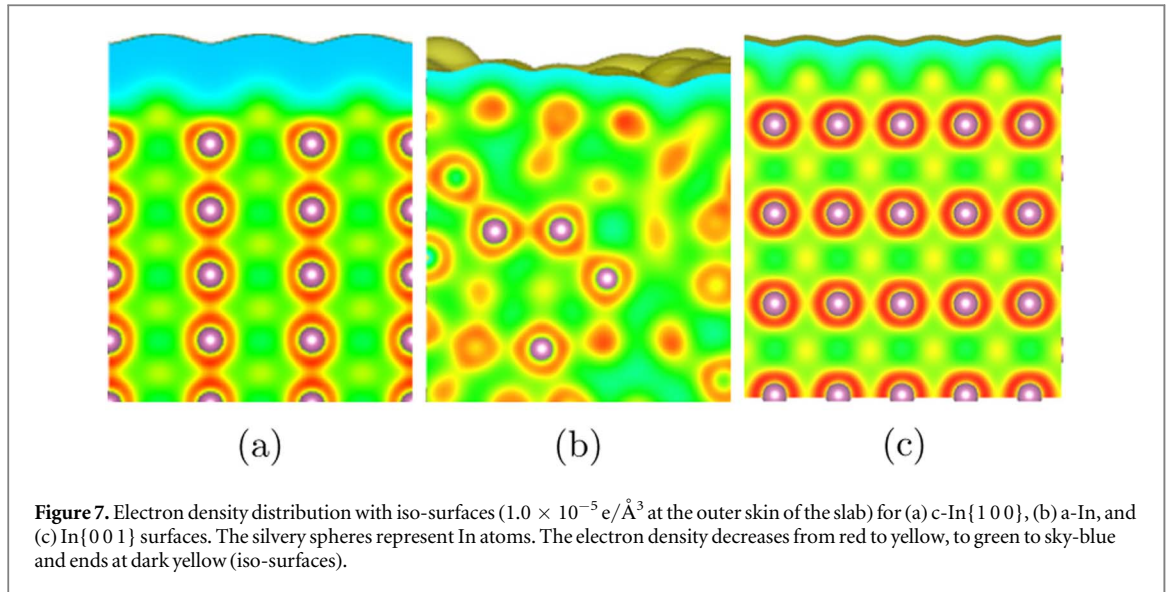
Figure 7 shows the electron-density distributions at the c-In surface (figures 7(c) and 7(c)) and at an a-In surface (figure 7(b)). The electron density decays quickly into the vacuum, reaching 10^{-5} e/Å^3 at a distance of ~6 Å from the surface. The electron density surfaces for In{0 0 1} and In{1 0 0} display a regular shape, whereas the electron density surface of a-In exhibit an irregular/disordered nature (figure 7(c)).

Based on the electron density distributions, we also obtained the average electrostatic potential for the In{0 0 1}, the In{0 0 1} and the a-In surfaces (figure 8). The local potentials of the In{0 0 1} and the In{1 0 0} exhibit ordering and periodicity whereas the local potentials of a-In show irregularities as well. However, at the surfaces the local potential converges to the vacuum potential quickly (about 7 Å from the surface). Moreover, the vacuum potentials of all surfaces differ moderately.

The electron work function (Φ) of a metal surface is the minimum energy needed to remove an electron from the bulk of a material via its surface to a point away from the material [54–56]. We define the work functions as follows:

$$\Phi = P_{vac} - E_F, \tag{2}$$

where P_{vac} is the local potential at vacuum and E_F is the Fermi level of the material. This equation was applied for the In{0 0 1}, the In{1 0 0} and the two a-In samples (in figure 8). The calculated work function is 3.90 eV for the In{0 0 1}, 3.77 eV for the In{1 0 0} and 3.82 eV for the a-In surfaces. The work-function being the same for the four a-In samples indicates that the thickness of the a-In slab is large enough. The larger work-function for the In{0 0 1} surface compared to the one for In{1 0 0} corresponds to the higher stability of the former one as well, as discussed before (table 1).
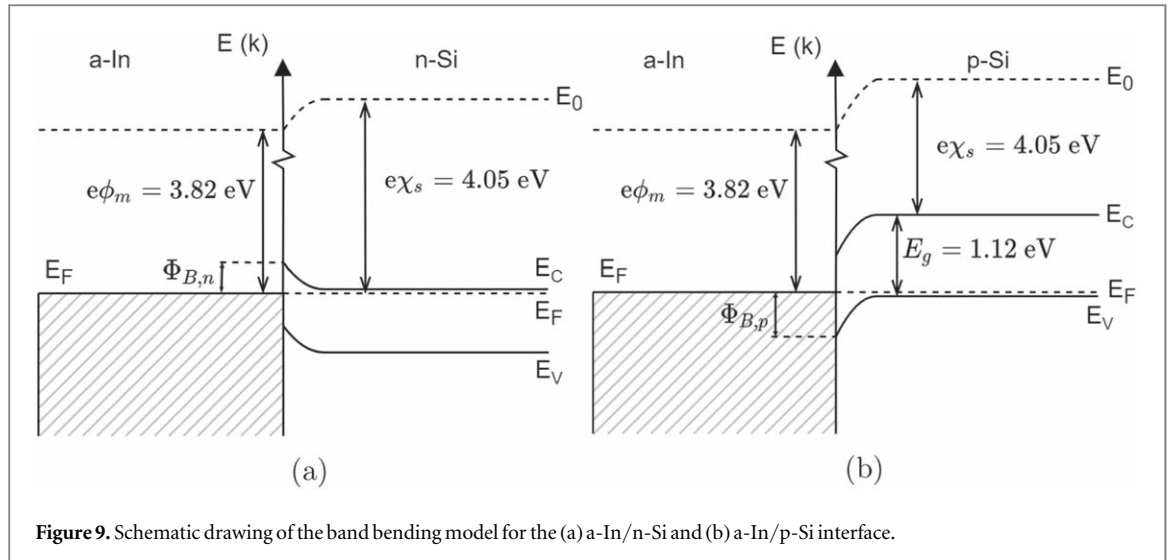
Figure 9. Schematic drawing of the band bending model for the (a) a-In/n-Si and (b) a-In/p-Si interface.

In literature, the experimental measurements for polycrystalline elemental In samples produced values ranging from 4.09–4.12 eV [55, 56]. The calculated values approach the experimental values, a remarkable feat considering the experimental difficulties in keeping the active In surfaces from being polluted (oxidation, etc).

4. Discussion: Schottky-Mott model and interfacial interaction

The present study revealed the formation of a distinct border between c-Si and a-In at the interfaces and strong chemical bonding between the interfacial Si and In atoms. At the c-Si/a-In interfaces, there are some states above the Fermi level in the pDOS of the interfacial Si atoms. This is similar to the metal induced gap states (MIGS) [31, 32]. There is charge transfer occurring from the interfacial In atoms to the Si atoms, resulting in the formation of Si^{-q}/In^{+q} barriers at the interfaces. The charge transfer originates from the electronegativity differences between Si (1.90 in Pauling scale) and In (1.78).

One expects that the negative charges at the interfacial Si atoms lead to induction of a hole-depletion region at the p-Si substrates. In analogy with the hypothesis in [18], according to which the observed depletion region in crystalline n-Si is associated with the inter-facial charge transfer from silicon to boron, here one can also expect the creation of a depletion region. Only in the case of the crystalline p-Si/a-In the negative charge at the interfacial silicon atoms lead to induction of a hole-depletion region in the p-Si substrate. Thus, crystalline p-Si/ a-In heterojunctions are expected to have rectifying effects as a Schottky-type diode. However we are not able to obtain the Schottky barrier height at present from our first principles approach [7, 19].

4.1. Schottky-Mott model of c-Si/a-In
The Schottky-Mott model has been widely used to study the Schottky barrier height (SBH) of metal-semiconductor junctions based on the work function of the metal (ϕ_m) and electron affinity of the semiconductor (χ_{Si}) [5, 7, 30, 37]. It is defined as follows:

$$\Phi_{B,n} = \phi_m - \chi_{Si} \tag{3a}$$

$$\Phi_{B,p} = (\chi_{Si} + E_g) - \phi_m. \tag{3b}$$

Here, $\Phi_{B,n/p}$ is the SBH for the n- and p-type semiconductor respectively and E_g is the energy gap of semiconductor. Equation (3a) is for a semiconductor with Fermi level pinned at the bottom of conduction band, e.g. n-Si, whereas equation (3b) is for a semiconductor with Fermi level pinned at the top of valence band, e.g. p-Si. With the calculated a-In work function and the experimental Si electron affinity and band gap [5, 7, 30, 37, 55, 57] we can apply the Schottky-Mott model.

According to figures 9(b) and (a) and the Schottky-Mott model [1], crystalline p-Si/a-In heterojunction is intrinsically a Schottky diode with a Schottky barrier height of $\Phi_{B,p} = \Delta E_g - (\Phi_M - \chi_{Si}) = 1.12 - (3.82 - 4.05) = 1.35$ eV for a very lightly doped p-Si and 1.25 when we assume Fermi level of Si is pinned slightly higher (0.1 eV) for a moderately doped Si. This result explains the rectifying phenomenon observed for the p-Si/In junctions [29]. Meanwhile, the Schottky barrier height is $\Delta\Phi_{B,n} = \phi_{In} - \chi_{Si} = 3.82 - 4.05 = -0.23$ eV for crystalline n-Si/a-In and thus, the junction should be ohmic-like [5, 7, 14, 15, 17]. We speculate that the formation of the ohmic-like junction corresponds with the charging of the interfacial Si at the c-Si/a-In interfaces.

Table 2. An overview of the averaged interfacial charge densities σ_e and distances between the charged Si^{-q} and In^{+q} plates d_{Si-In}. The consequent potentials ΔP from the parallel-plates charge model and the SBH $\Delta\Phi_{SBH}$ from the Schottky-Mott model for n-Si/a-In were obtained using equation (4), (3a) and (3b) respectively.

Interface	σ_{atom}(Si/m^2)	σ_e(C/m^2)	d_{Si-In}(m)	ΔP(eV)	$\Delta\Phi_{SBH}$(eV)
Si{0 0 1}/a-In	6.78×10^{18}	-0.25	1.7×10^{-10}	-0.42	-0.23
Si{1 1 1}/a-In	7.83×10^{18}	-0.10	2.6×10^{-10}	-0.37	

4.2. Fermi level pinning and SBH at the c-Si/a-In interface

Here we try to analyze the relations between the atomic picture from the *ab initio* study and the macroscopic Schottky-Mott approximation.

The present study provided us an atomic picture of the heterojunctions with information about their local atomic structure, chemical bonding, charges at and charge transfer between interfacial atoms. Moderate charge transfer occurs from In to Si (-0.23e/Si) at Si{0 0 1}/a-In and (-0.08 e/Si) at Si{1 1 1}/a-In, forming interfacial Si^{-q}/a-In^{+q} charge barriers. The charge transfer is essentially confining the outer atomic layer (of both a-In and c-Si). Hence we attempt to model its effect as a dipole layer, i.e. a parallel plate 'capacitor' with the charge density determined by the amount of electrons transferred from In to Si and where the plates are separated by the average interfacial Si-In distance d_{Si-In} (table 2).

In order to estimate the charge barrier heights based on the *ab initio* approach, we use a simple parallel-plates model. The potential difference ΔP is proportional to the amount of charge at the plates and distance d between the plates:

$$\Delta P = \int E(z)\,dz = E \times d = \frac{\sigma e \times d}{\epsilon\,(Si)} \tag{4}$$

here $\sigma e = Q/A$ is the charge density of the plates with Q the charge at the area of the plate (A); d is the distance between the plates, which is an average of the interfacial Si-In bonds lengths, $\epsilon(Si) = \epsilon_0 \times \epsilon_r(Si)$ with $\epsilon_0 = 8.854 \times 10^{-12}$ F/m and $\epsilon_r(Si) = 11.7$ is the dielectric constant of Si, considering that mobile electrons moving from n-Si through the nearby region. The calculated charge barriers according to equation (4) are in table 2. The calculations also showed effect of cystalline anisotropy of the Si substrates that the n-Si{0 0 1}/a-In has a large potential barrier than that at n-Si{1 1 1}/a-In. Furthermore, we obtained the SBH via the Schottky-Mott model for n-Si/a-In equation (3a): -0.23 eV. Therefore, the charge barriers' values in table 2 is in line with that from the Schottky-Mott model. Such agreement is understandable since both interfacial charge transfer and difference between work-function of a metal and vacuum electron affinity of a n-type semiconductor at the contact originate from the capability of the components to attract electrons— better known as the electronegativity of the elements [57].

For p-Si/a-In, the Fermi level at the hole-depletion zone is at top of the valence band. Electrons must be excited to the conduction band first to become mobile. Moreover, the conduction electrons must overcome the charge barrier. Thus, the overall barrier is determined by the difference of the Si bandgap ($\sim$1.12 eV at room temperature) and the charge barriers in table 2. The barrier is 1.64 eV for p-Si{0 0 1}/a-In and 1.35 eV for p-Si{1 1 1}/a-In. These values are close to the value obtained from equation (3b), 1.37 eV.

Another issue is about the influence of electrons into the depletion zone on the charge barriers. We assume a complete depletion with a width of 8 μm with a doping concentration of 1×10^{16} e/cm^3, which is typical in practice [18]. Then $q_{dep} = 1 \times 10^{16}$ e/cm$^3 \times 8\mu$m $= 4 \times 10^{12}$ e/cm^2 if we assume a linear decay model.

The Si density at the Si surfaces is about 6.78×10^{14} atoms/cm^2 (table 2). The change in charge at the interface can be calculated: $(4\times10^{12}$ e/cm$^2)/(6.78 \times 10^{14}$ atoms/cm$^2)$ $\sim$0.006 e/Si for a complete depletion, which is notably smaller than the interfacial charge $\sim$0.23 e/Si at Si{0 0 1}/a-In or 0.08 e/Si at Si{1 1 1}/a-In (table 2). This amount of change is notably smaller than the interfacial charge. Therefore, we believe that this effect for low- and moderately doped Si substrates are not significant.

5. Conclusions

In this work we investigated the c-Si/a-In interfaces using both AIMD simulation and the Schottky-Mott model. The AIMD study revealed i) clear borders between c-Si and a-In at the interfaces with surficial Si atoms bonding to adjacent In, which satisfy the tetragonal coordination of Si; ii) the a-In atoms adjacent to the Si{1 1 1} substrate exhibit more pronounced layering than those on the Si{0 0 1} substrate; iii) there is charge transfer from the interfacial In to Si, resulting in the formation of c-Si^{-q}/a-In^{+q} charge barriers. The negatively charging of the interfacial Si induces hole-depletion regions in the p-Si regions. Thus, the c-p-Si/a-In heterojunction acts intrinsically as a rectifying diode, whereas c-n-Si/a-In creates an ohmic contact, in agreement with the previous

experimental observations. The information obtained here is helpful in the development of new Si/In heterojunctions.

Based on the Schottky-Mott approximation, we find that the crystalline p-Si/a-In junction is a Schottky barrier with a Schottky barrier height of ~1.3 eV, whereas crystalline n-Si/a-In has no rectifying properties. Thus, the two approaches agree with each other via the pinning position of the Fermi level at the electron-/hole-depletion zones.

Our study shows that at first order of approximation the potential barrier resulting from the charge transfer between interfacial silicon and indium (we call it 'charge barrier') is representative of the potential difference between the work function of the metal electron affinity or the ionization potential (electron affinity plus the band gap) of the semiconductor. This study further reveals a necessity to develop more desirable approaches, including advanced *ab initio* methods to obtain accurate information about the heterojunctions.

Acknowledgments

Data availability statement

All data that support the findings of this study are included within the article (and any supplementary files).

ORCID iDs

Stoyan Nihtianov ⓘ https://orcid.org/0000-0001-9937-8510
Paolo Sberna ⓘ https://orcid.org/0000-0001-6156-1125
Gilles A de Wijs ⓘ https://orcid.org/0000-0002-1818-0738
Changming Fang ⓘ https://orcid.org/0000-0003-0915-7453

References

[1] Sarubbi F, Nanver L K and Scholters L M 2010 High effective Gummel number of CVD boron layers in ultrashallow p + n diode configurations *IEEE Trans Electron Devices* **57** 1269–78

[2] Shi L *et al* 2010 Optical performance of B-layer ultra-shallow-junction silicon photodiodes in the VUV spectral range *Procedia Eng* **5** 633–6

[3] Mohammadi V, De Boer W B and Nanver L K 2012 Temperature dependence of chemical-vapor deposition of pure boron layers from diborane *Appl Phys Lett* **101** 111906

[4] Sarubbi F, Nanver L K and T L Scholtes 2006 CVD delta-doped boron surface layers for ultra-shallow junction formation *ECS Trans* **3** 35–44

[5] Tersoff J 1984 Theory of semiconductor heterojunctions: the role of quantum dipoles *Phys Rev B* **30** 4874–7

[6] Aberle A G 2000 Surface passivation of crystalline silicon solar cells: a review *Prog Photovoltaics Res Appl* **8** 473–87

[7] Tung R T 2014 The physics and chemistry of the Schottky barrier height. *Appl Phys Rev* **1** 011304

[8] Lamers M *et al* 2014 The interface of a-SiNx:H and Si: linking the nano-scale structure to passivation quality *Sol Energ Mat Sol* **120** 311–6

[9] Nanver L K *et al* 2012 (Invited) Pure dopant deposition of B and Ga for ultrashallow junctions in Si-based devices *ECS Trans* **49** 25–33

[10] Sammak A 2012 Silicon-based integration of groups III, IV, V chemical vapor depositions in high-quality photodiodes *PhD Thesis* TU Delft

[11] Greenwood N N 1997 *Chemistry of the elements.* (Oxford Boston: Butterworth- Heinemann)

[12] Arblaster J 2018 Selected values of the crystallographic properties of elements *Materials Park: A S M International*

[13] Mostafa A and Medraj M 2017 Binary phase diagrams and thermodynamic properties of silicon and essential doping elements (Al, As, B, Bi, Ga, In, N, P, Sb and Tl) *Materials* **10** 676

[14] Robertson J 2005 High dielectric constant gate oxides for metal oxide Si transistors *Rep Progr Phys* **69** 327–96

[15] Cowley A M and Sze S M 1965 Surface states and barrier height of metalsemiconductor systems *J Appl Phys* **36** 3212–20

[16] Brillson L J 1978 Transition in Schottky barrier formation with chemical reactivity *Phys Rev Lett* **40** 260–3

[17] Mönch W 1994 Metal-semiconductor contacts: electronic properties *Surf Sci 299* **300** 928–44

[18] Mohammadi V, Nihtianov S and Fang C M 2017 A doping-less junction-formation mechanism between n-silicon and an atomically thin boron layer *Sci Rep* **7** 13247

[19] Fang P X *et al* 2021 Interfaces between crystalline Si and amorphous B: interfacial interactions and charge barriers *Phys Rev B* **103** 075301

[20] Sberna P *et al* 2021 Mechanism of electronegativity heterojunction of nanometer amorphous-boron on crystalline silicon: an overview *Crystals* **11** 108

[21] Lander J J and Morrison J 1965 Surface reactions of silicon (111) with aluminum and indium *J Appl Phys* **36** 1706–13

[22] Raj V, Chauhan A K S and Gupta G 2015 Growth kinetics of indium metal atoms on Si(1 1 2) surface *Mater Res Bull* **72** 286–90

[23] Chou J P *et al* 2014 Atomic structure and electronic properties of the In/Si(111)22 surface *Phys Rev B* **89** 155310

[24] Kwon S G and Kang M H 2014 Honeycomb network of indium trimers and monomers on Si(111)-(22) *Phys Rev B* **89** 165304

[25] Teubner T *et al* 2012 Growth kinetics on silicon facets during low-temperature crystallization from indium solution *J Cryst Growth* **347** 31–6

[26] Zhang T *et al* 2010 Superconductivity in one-atomic-layer metal films grown on Si(111) *Nat Phys* **6** 104–8

[27] Vlachos D *et al* 2010 Indium growth on reconstructed Si(111) $\sqrt{3} \times \sqrt{3}$ and 4 × 1 in surfaces *The Journal of Physical Chemistry C* **114** 17693–702

[28] Park J W and Kang M H 2016 Single-layer limit of metallic indium overlayers on Si(111) *Phys Rev Lett* **117** 116102

[29] Migitaka M and Tokuyama T 1966 Method of manufacturing silicon diodes or silicon transistors by alloying indium with p-type silicon to produce a p-n junction *US3285791A*.

[30] Tung R T 2000 Chemical bonding and Fermi level pinning at metal-semiconductor interfaces *Phys Rev Lett* **84** 6078–81

[31] Louie S G and Cohen M L 1975 Self-consistent pseudopotential calculation for a metal-semiconductor interface *Phys Rev Lett* **35** 866–9

[32] Louie S G, Chelikowsky J R and Cohen M L 1976 Theory of semiconductor surface states and metal-semiconductor interfaces *J Vac Sci Technol* **13** 790–7

[33] Tang Y *et al* 2022 First-principle studies on the metal/semiconductor properties and strain-tuned electronic structures of SnP3 monolayer *Comput. Mater. Sci.* **203** 111047

[34] Urquiza M L and Cartoix`a X 2020 Schottky barriers, emission regimes and contact resistances in 2H-1T' MoS2 lateral metal-semiconductor junctions from firstprinciples *2D Materials* **7** 045030

[35] Perrine K A and Teplyakov A V 2010 Reactivity of selectively terminated single crystal silicon surfaces *Chem Soc Rev* **39** 3256

[36] Andrews J M and Phillips J C 1975 Chemical bonding and structure of metal/semiconductor interfaces. C R C Critical Reviews in *Solid State Sci.* **5** 405–8

[37] Robertson J 2009 Band alignment at metal-semiconductor and metal-oxide interfaces *Phys Status Solidi A* **207** 261–9

[38] Hintzsche L E *et al* 2012 Density functional theory study of the structural and electronic properties of amorphous silicon nitrides: Si3N4-x:H *Phys Rev B* **86** 235204

[39] Fang C M and Fan Z 2020 Atomic ordering at the interfaces between liquid Al and solid MgO: an ab initio molecular dynamics study *Philos. Mag. Lett.* **100** 235–44

[40] Kresse G and Hafner J 1994 Ab initio molecular-dynamics simulation of the liquidmetal- amorphous-semiconductor transition in germanium *Phys Rev B* **49** 14251–69

[41] Bl¨ochl P E 1994 Projector augmented-wave method *Phys Rev B* **50** 17953–79

[42] Kresse G and Joubert D 1999 From ultrasoft pseudopotentials to the projector augmented-wave method *Phys Rev B* **59** 1758–75

[43] Perdew J P, Burke K and Ernzerhof M 1996 Generalized gradient approximation made simple *Phys Rev Lett* **77** 3865–8

[44] Monkhorst H J and Pack J D 1976 Special points for brillouin-zone integrations *Phys Rev B* **13** 5188–92

[45] Wyckoff R W G 1963 *Crystal Structures* (New York: Interscience Publishers)

[46] Bludau W, Onton A and Heinke W 1974 Temperature dependence of the band gap of silicon *J Appl Phys* **45** 1846–8

[47] Jones R O 2015 Density functional theory: its origins, rise to prominence, and future *Rev Mod Phys* **87** 897–923

[48] Pauling L 1931 The nature of the chemical bond *Application of results obtained from the quantum mechanics and from a theory of paramagnetic susceptibility to the structure of molecules. J Am Chem Soc* **53** 1367–400

[49] Fang C M, Men H and Fan Z 2018 Effect of substrate chemistry on prenucleation *A* **49** 6231–42

[50] Hashibon A *et al* 2002 Atomistic study of structural correlations at a liquid-solid interface *Comput Mater Sci* **24** 443–52

[51] Wang Y and Hamers R J 1995 Boron-induced reconstructions of Si(001) investigated by scanning tunneling microscopy *Journal of Vacuum Science & Technology A: Vacuum, Surfaces, and Films* **13** 1431–7

[52] Fang C M *et al* 2020 Stability, geometry and electronic properties of BHn (n=0 to 3) radicals on the Si0 0 131:H surface from first-principles *J Phys: Condens Matter* **32** 235201

[53] Bader R F W 1991 A quantum theory of molecular structure and its applications *Chem Rev* **91** 893–928

[54] Singh-miller N E and Marzari N 2009 Surface energies, work functions, and surface relaxations of low-index metallic surfaces from first principles *Phys Rev B* **80** 235407

[55] Michaelson H B 1977 The work function of the elements and its periodicity *J Appl Phys* **48** 4729–33

[56] Grundmann M 2010 The physics of semiconductors *Springer-Verlag GmbH*

[57] Michaelson H B 1978 Relation between an atomic electronegativity scale and the work function *IBM J. Res. Dev.* **22** 72–80